THE JOURNAL OF PHYSICAL CHEMISTRY LETTERS
A JOURNAL OF THE AMERICAN CHEMICAL SOCIETY

pubs.acs.org/JPCL

Letter

Inverse Design of Next-Generation Superconductors Using Data-Driven Deep Generative Models

Daniel Wines,* Tian Xie, and Kamal Choudhary

Cite This: J. Phys. Chem. Lett. 2023, 14, 6630−6638

Read Online

ACCESS | Metrics & More | Article Recommendations | Supporting Information

ABSTRACT: Finding new superconductors with a high critical temperature (T_c) has been a challenging task due to computational and experimental costs. We present a diffusion model inspired by the computer vision community to generate new superconductors with unique structures and chemical compositions. Specifically, we used a crystal diffusion variational autoencoder (CDVAE) along with atomistic line graph neural network (ALIGNN) pretrained models and the Joint Automated Repository for Various Integrated Simulations (JARVIS) superconducting database of density functional theory (DFT) calculations to generate new superconductors with a high success rate. We started with a DFT data set of ∼1000 superconducting materials to train the diffusion model. We used the model to generate 3000 new structures, which along with pretrained ALIGNN screening results in 61 candidates. For the top candidates, we performed DFT calculations for validation. Such approaches go beyond funnel-like materials screening approaches and allow for the inverse design of next-generation materials.

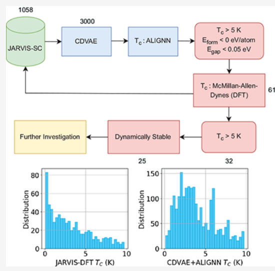

After superconductivity was discovered in 1911 by Onnes,[1] the efforts to identify novel superconducting materials with high transition temperatures (T_c) has been an intense area of research in materials science and condensed matter physics.[2,3] There have been systematic computational efforts to identify Bardeen−Cooper−Schrieffer (BCS) conventional superconductors[4,5] with high T_c prior to costly experimental investigation,[6−8] where density functional theory-perturbation theory (DFT-PT) calculations have been performed to obtain the electron−phonon coupling (EPC) parameters. In addition, various machine learning approaches have been utilized to accelerate the search for high-T_c superconductors.[6,9−14] However, these typical funnel-like screening-based approaches are not sufficient for inverse materials design, where, instead of engineering from structure to property, the goal is to engineer from a target property to the crystal structure.

The inverse design of novel materials becomes a difficult problem to solve because there are an infinite number of possible materials with varying properties that are dependent on chemical composition and crystal structure. In order for inverse design to be successful, an algorithm that can successfully create new candidate structures based on a high quality and diverse data set of materials data is required. There currently exists abundant sources of high quality calculated material properties in databases such as Materials Project,[15] Open Quantum Materials Database (OQMD),[16,17] C2DB,[18,19] and our own JARVIS[20] database, which all contain millions of high-throughput[20,21] DFT calculations. The main obstacle in inverse design has been the method or algorithm used to generate new candidate materials. To circumvent this obstacle, generative machine learning algorithms can be used to design new candidate structures. With the popularity of generative tools such as DALL-E,[22] which uses deep learning models to generate digital images from natural language descriptions (prompts), the interest in using deep generative models for scientific applications has immensely increased.[23−26] One of the main challenges with generative models for periodic materials stems from the creation of representations that are translationally and rotationally invariant.[27−34]

In a recent work, Xie et al. developed a crystal diffusion variational autoencoder (CDVAE) model[24] (https://github.com/txie-93/cdvae) for periodic structure generation. The CDVAE consists of a variational autoencoder[35] and a diffusion model[36−38] that works directly with the atomic coordinates of the structures and uses an equivariant graph neural network[39] to ensure invariance without the need for representations such as graphs or descriptors. The CDVAE consists of three simultaneously trained networks: (1) the encoder, which encodes onto the latent space, (2) the property predictor, which samples the latent space and predicts a structure and composition, and (3) the decoder, which is a diffusion model that denoises the randomly initialized atom types into a material that is similar to the training set distribution. More details of the CDVAE method can be found in Xie et al.[24] A recent work by Lyngby and Thygesen[25] successfully applied the CDVAE model to discover new, stable 2D materials and vastly expand the space of 2D materials (on the order of thousands). Another recent work by Moustafa et al.[26] used the

Received: May 13, 2023
Accepted: July 12, 2023

https://doi.org/10.1021/acs.jpclett.3c01260
J. Phys. Chem. Lett. 2023, 14, 6630−6638

CDVAE model to discover more than 500 new stable one-dimensional materials. In this work, we trained a CDVAE model (optimizing T_c in the latent space) with DFT computed data of 1058 superconducting materials from the JARVIS database and generated thousands of new candidate superconductors. We screened these candidate structures further by predicting the properties using pretrained deep learning models for fast predictions. After narrowing down the pool of potential candidate superconductors, we performed DFT calculations to verify our predictions and assessed the dynamic and thermodynamic stabilities of the newly predicted materials.

We utilized the atomistic line graph neural network (ALIGNN)[40] (https://github.com/usnistgov/alignn) to make deep learning predictions of the superconducting properties of each material. This pretrained model for superconducting properties was specifically developed in ref 6. ALIGNN is implemented in the deep graph library[41] and PyTorch.[42] In the ALIGNN framework, a structure is represented as a graph, where the elements are nodes and bonds are edges. Nine input features are assigned to each node in the graph. These features include the first ionization energy, electron affinity, electronegativity, block, valence electrons, group number, covalent radius, and atomic volume. The edge features are the bond distances where the cutoff for the radial basis function is 8 Å. A 12-nearest-neighbor periodic graph construction is used. The line graph is constructed from the atomistic graph, using bond distances as nodes and bond angles as edge features. Edge-gated graph convolution is used for updating the nodes and edge features by the use of a propagation function. An edge-gated graph convolution on the bond graph with an edge-gated convolution on the line graph is what composes one layer. Bond messages are produced from the line graph convolution that is propagated to the atomistic graph, where the bond features and atom features are further updated. With regard to predicting superconducting properties, we used a batch size of 16, 90:5:5 split, and training for 300 epochs, where the test set was not used at all during training. We kept the hyperparameters of the model the same as the original ALIGNN paper.[40]

We utilize the publicly available JARVIS[20] infrastructure for our DFT and deep learning goals mentioned above. JARVIS (Joint Automated Repository for Various Integrated Simulations, https://jarvis.nist.gov/) is a collection of databases and tools to automate materials design using classical force-field, density functional theory, machine learning calculations, and experiments. JARVIS-DFT is a density functional theory based database of over 75,000 materials with several material properties such as formation energy, band gap with different levels of theory,[43] solar-cell efficiency,[44] topological spin−orbit coupling spillage,[45−47] elastic tensors,[48] dielectric tensors, piezoelectric tensors, infrared and Raman spectra,[49] electric field gradients,[50] exfoliation energies,[51] two-dimensional (2D) magnets,[52] and bulk[6] and 2D superconductors,[7] all with stringent DFT-convergence setup.[53] Our ALIGNN and CDVAE models were trained on the 1058 DFT calculations of superconducting properties presented in ref 6.

To verify top candidate superconductors, we followed the workflow used to generate the training data (in ref 6), where we performed EPC calculations using non-spin-polarized DFT-PT[54,55] (using the interpolated/Gaussian broadening method[56]) with the Quantum Espresso (QE) software package,[57] PBEsol functional,[58] and the GBRV[59] pseudopotentials. The EPC parameter is derived from spectral function $\alpha^2F(\omega)$ which is calculated as follows

$$\alpha^2F(\omega) = \frac{1}{2\pi N(\epsilon_F)} \sum_{qj} \frac{\gamma_{qj}}{\omega_{qj}} \delta(\omega - \omega_{qj}) w(q) \tag{1}$$

where ω_{qj} is the mode frequency, $N(\epsilon_F)$ is the DOS at the Fermi level ϵ_F, δ is the Dirac-delta function, $w(q)$ is the weight of the q point, and γ_{qj} is the line width of a phonon mode j at wave vector q and is given by

$$\gamma_{qj} = 2\pi\omega_{qj} \sum_{nm} \int \frac{d^3k}{\Omega_{BZ}} |g^j_{kn,k+qm}|^2 \delta(\epsilon_{kn} - \epsilon_F) \delta(\epsilon_{k+qm} - \epsilon_F) \tag{2}$$

Here, the integral is over the first Brillouin zone, ϵ_{kn} and ϵ_{k+qm} are the DFT eigenvalues with wavevector k and $k + q$ within the nth and mth bands, respectively, and $g^j_{kn,k+qm}$ is the electron−phonon matrix element. γ_{qj} is related to the mode EPC parameter λ_{qj} by

$$\lambda_{qj} = \frac{\gamma_{qj}}{\pi h N(\epsilon_F) \omega_{qj}^2} \tag{3}$$

Now, the EPC parameter is given by

$$\lambda = 2 \int \frac{\alpha^2F(\omega)}{\omega} d\omega = \sum_{qj} \lambda_{qj} w(q) \tag{4}$$

with $w(q)$ as the weight of a q point. The superconducting transition temperature, T_c, can then be approximated using the McMillan−Allen−Dynes[60] equation as follows:

$$T_c = \frac{\omega_{\log}}{1.2} \exp\left[-\frac{1.04(1 + \lambda)}{\lambda - \mu^*(1 + 0.62\lambda)}\right] \tag{5}$$

where

$$\omega_{\log} = \exp\left[\frac{\int d\omega \frac{\alpha^2F(\omega)}{\omega} \ln \omega}{\int d\omega \frac{\alpha^2F(\omega)}{\omega}}\right] \tag{6}$$

In eq 5, the parameter μ^* is the effective Coulomb potential parameter, which we take as 0.1. It is important to note that the robustness of this workflow was heavily benchmarked against experimental data and higher levels of theory in refs 6 and 7, which indicates that the training data for these deep learning models is of high quality, given the level of theory used to produce the data.

The full inverse design workflow proposed in this work is depicted in Figure 1a. The first step of this workflow involved training the CDVAE model on the 1058 DFT calculations in the JARVIS-SC (superconducting) database (from ref 6). With regard to the CDVAE model for inverse design, the target property to optimize was T_c for new candidate superconductors. After training on the JARVIS-SC data, we generated 3000 candidate materials using the CDVAE model, where T_c was optimized in the latent space. To ensure that the CDVAE model optimized T_c in the latent space and actually "learned" superconductivity from the JARVIS-SC training data, we analyzed the property loss function (which is depicted in Figure S1). As seen in Figure S1, the loss function is sharply decreasing and converging around 1.2 K. This converged value is comparable to the mean absolute error

https://doi.org/10.1021/acs.jpclett.3c01260
J. Phys. Chem. Lett. 2023, 14, 6630−6638

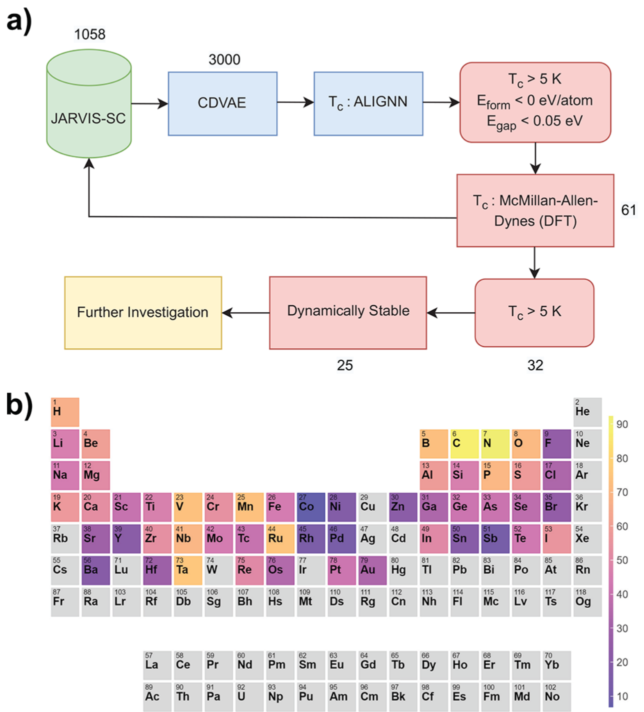

Figure 1. (a) The full inverse design workflow for new superconductors using DFT, ALIGNN, and the CDVAE generative model and (b) the probability that compounds containing a given element in the CDVAE generated structures have an ALIGNN predicted T_c > 3 K.

(MAE) achieved in the ALIGNN model for T_c reported in ref 6.

With such a large amount of crystal structures to investigate, it is impractical to perform DFT calculations of the EPC workflow for all of the candidates. For this reason, we used our deep learning property prediction tool (ALIGNN) to screen all 3000 candidate materials. ALIGNN has demonstrated success for predicting properties such as formation energy and band gap and more recently superconducting T_c. The screening criteria we established for further investigation of these candidates was ALIGNN predicted: T_c > 5 K, E_{form} < 0 eV/atom, and E_{gap} < 0.05 eV. This criterion is based on the fact that we want to further investigate superconducting materials which have a high T_c, are potentially stable, and are metallic (high density of states at the Fermi level). Although negative formation energy is a stringent requirement for stability, investigations of dynamic and thermodynamic stability are still needed to confirm stability (phonon spectrum and energy above the convex hull). After performing this screening with ALIGNN, we found 61 materials that fit this criterion. We then went on to perform the full DFT-EPC workflow for these 61 materials and computed the T_c using the McMillan–Allen–Dynes equation. After computing the T_c of these materials with DFT, we found that 32 structures have a T_c above 5 K. Upon investigation of the phonon density of states and chemical composition, we find that 7 of these structures have negative phonon frequencies, indicating dynamical instability. The remaining 25 candidate superconductors are listed in Table 1.

Before discussing the more detailed results of the 25 new candidate superconducting materials generated by our workflow (shown in Figure 1a), we will discuss the intermediate steps of the workflow in more detail. The CDVAE model has the capability to produce new structures with chemical and structural diversity. Figure 1b depicts the probability that compounds containing a given element in the 3000 CDVAE generated structures have an ALIGNN predicted T_c above 3 K (displayed as a heat map overlaid on the periodic table). We observe that compounds containing C, N, B, O, V, Mn, Nb, Ru, and Ta are the most abundant with regard to structures that have a higher predicted T_c with ALIGNN. This is not surprising due to the fact that several of the materials in the DFT training set that have a high value of T_c contain such elements (see ref 6 for details).

Table 1. Chemical Formula, JARVIS ID (JID), T_c, Formation Energy per Atom, and Energy above the Convex Hull per Atom of the 25 Candidate Superconductors from CDVAE Verified by DFT Calculations

Structure	JID	T_c (K)	E_{form} (eV/atom)	E_{hull} (eV/atom)
VN_2	JVASP-161655	20.2	−0.56	0.32
NTaB (I)	JVASP-161630	16.2	−0.32	0.84
BORu	JVASP-161610	12.4	−0.72	0.75
BTa_2N	JVASP-161612	11.9	−0.37	0.67
MnN	JVASP-161621	11.4	−0.43	0.01
NTaB (II)	JVASP-161624	11.1	−0.32	0.84
VN	JVASP-161656	9.6	−0.98	0.34
BN_2Zr	JVASP-161608	9.3	−1.23	0.43
BTaNS	JVASP-161613	9.1	−0.33	0.88
NP_2Sr	JVASP-162663	8.4	−0.54	0.22
TaP_2	JVASP-161649	8.1	−0.45	0.25
AlN_2Zr	JVASP-161600	7.8	−1.40	0.39
$NPdTi_2$	JVASP-161629	7.7	−0.78	0.47
$PScSi_2$	JVASP-161644	7.4	−0.43	0.49
NbRh	JVASP-161638	7.4	−0.41	0.00
AlN_2V (I)	JVASP-161599	7.2	−1.14	0.34
TiO_2NbN	JVASP-161653	7.1	−2.15	0.30
NBaP	JVASP-161626	6.6	−0.59	0.22
NVBRu	JVASP-161631	6.3	−0.14	0.74
ScO_3Zr	JVASP-161647	6.3	−3.43	0.15
Al_2N	JVASP-161597	5.9	−0.79	0.31
AlN_2V (II)	JVASP-162662	5.4	−1.14	0.34
TiN	JVASP-161652	5.3	−1.56	0.35
ScBORuCa	JVASP-161646	5.2	−1.12	0.58
B_2TaS	JVASP-161604	5.2	−0.07	0.58

Although the abundance of elements in the CDVAE structures (with an ALIGNN predicted T_c > 3 K) follows trends similar to those in the training data, the CDVAE candidate structures are not restricted to stoichiometries and crystal structures already present in the training data. This is illustrated by Figure 2, where the chemical formula, distribution of densities, and distribution of packing fractions for (a−c) the 3000 CDVAE generated structures and for (d−f) the 1058 structures used for training from the JARVIS-DFT database are depicted. A comparison of Figure 2a and d emphasizes the difference in the stoichiometry between the CDVAE generated structures and the training data from JARVIS. For example, in the JARVIS training set, a majority of the data contains only three different atomic species (A, B, and C) and the unit cells have 5 formula units (see Figure 2d). In contrast, the CDVAE generated data based on the JARVIS training set (see Figure 2a) has a number of structures that contain four atomic species (A, B, C, D) and unit cells that have a larger number of formula units (i.e., AB_7). In addition,

https://doi.org/10.1021/acs.jpclett.3c01260
J. Phys. Chem. Lett. 2023, 14, 6630−6638

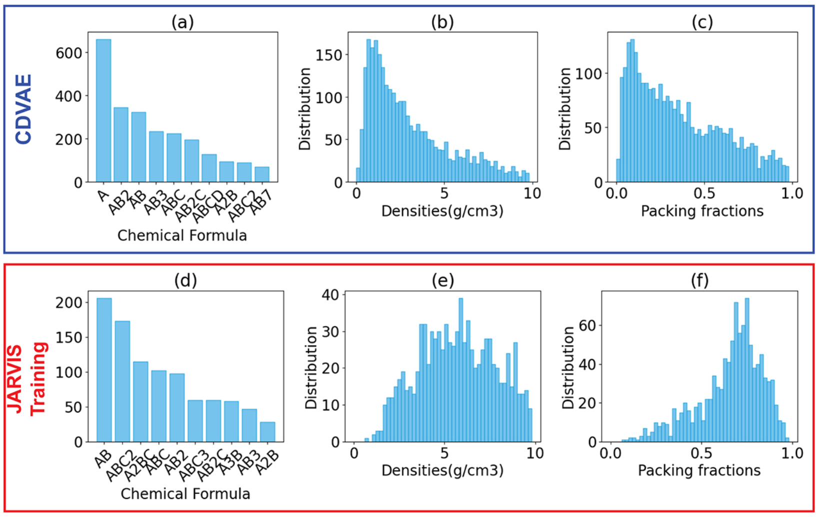

Figure 2. Chemical formula, distribution of densities, and distribution of packing fractions for (a−c) the 3000 CDVAE generated structures and (d−f) the 1058 structures used for training from the JARVIS-DFT database.

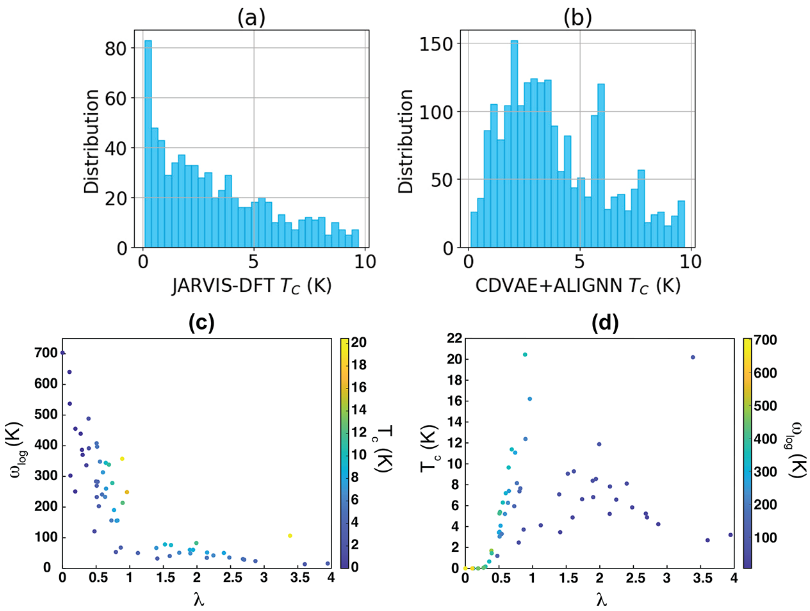

Figure 3. Distribution of T_c for the (a) 1058 JARVIS-DFT structures (T_c computed with DFT) and (b) the 3000 CDVAE structures (T_c computed with ALIGNN). (c, d) Relationship between EPC parameters for the CDVAE candidate materials verified with DFT.

the CDVAE generated data contains a substantial number of monoelemental structures, while this is not a prevalent component in the training set. When comparing Figure 2b,e and c,f, we observe very different distributions for densities and packing fractions between the CDVAE structures and JARVIS training data. Specifically, the CDVAE generated structures have a much larger distribution of structures with a low density and packing fraction. This can be due in part to the low symmetry of the CDVAE generated structures, which gives rise to larger crystal volumes for the newly generated unit cells and, therefore, smaller densities and packing fractions. In fact, the CDVAE structures are all in space group P1. The likelihood of the CDVAE model generating low symmetry, chemically diverse structures might be attributed to the CDVAE model sampling from a Gaussian distribution to create new materials (to predict the number of atoms and composition). Since the underlying distribution of the materials is non-Gaussian and the Gaussian distribution that the CDVAE model samples from is not representative of the latent space, materials out of the distribution can be generated. This is a limitation of CDVAE that could be addressed with a better latent space encoding in the future.

After discussing the structural and chemical diversity of the CDVAE generated structures, we plan to discuss the steps of the workflow that involve the prediction of T_c with deep learning (ALIGNN) and DFT. The ALIGNN deep learning property predictor for T_c was previously pretrained on the data set in ref 6 (1058 materials) and benchmarked. Using the pretrained ALIGNN model allows us to filter the vast amount of CDVAE candidate superconductors with instantaneous property prediction. Figure 3a and b depicts the distribution of T_c for the (a) 1058 JARVIS-DFT structures (T_c computed with DFT) and (b) the 3000 CDVAE structures (T_c computed with ALIGNN). As seen in the figure, the distribution of T_c is vastly different. Most strikingly, the CDVAE generated data has a very low amount of structures with a predicted T_c close

https://doi.org/10.1021/acs.jpclett.3c01260
J. Phys. Chem. Lett. 2023, 14, 6630−6638

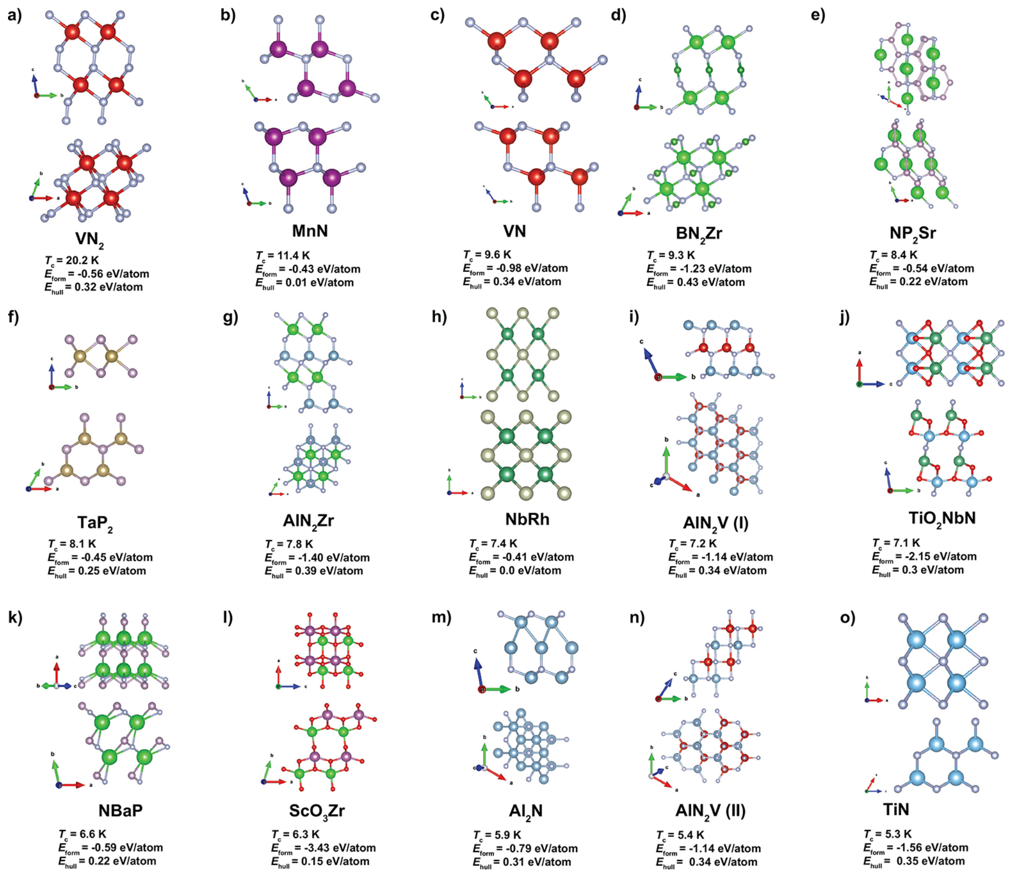

Figure 4. Top and side views of the top superconductor candidates (closest to the convex hull) generated with CDVAE and verified with DFT: (a) VN_2, (b) MnN, (c) VN, (d) BN_2Zr, (e) NP_2Sr, (f) TaP_2, (g) AlN_2Zr, (h) NbRh, (i) AlN_2V (I), (j) TiO_2NbN, (k) NBaP, (l) ScO_3Zr, (m) Al_2N, (n) AlN_2V (II), and (o) TiN. T_c, E_{form}, and E_{hull} are also given for each material.

to zero (non-superconducting), as opposed to a large number of materials in the JARVIS training set that have a T_c value close to zero. In addition, the distribution of CDVAE +ALIGNN temperatures resembles more of a Gaussian distribution, with a majority of the T_c values of the newly generated structures concentrated around 2.5−6 K. This can be an indicator of the success of the CDVAE model for generating new structures with an optimized target property, such as T_c, in the latent space.

After screening the 3000 CDVAE generated structures with ALIGNN, we performed DFT for the 61 candidates that met the ALIGNN screening criteria depicted in Figure 1a. At this stage, it is important to acknowledge the success of the pretrained ALIGNN model with regard to predicting the T_c values of these newly generated structures. Out of the 61 structures, 54 of them have a DFT computed $T_c > 0.5$ K, which indicates that ALIGNN is 89% successful with filtering out superconducting materials from the CDVAE generated structures. Out of the 61 structures, 32 of them have a DFT computed $T_c > 5$ K, which indicates that ALIGNN has a 52% success rate in filtering out materials with a T_c above 5 K from the CDVAE generated structures. More details of the ALIGNN screening are given in the Supporting Information. It is important to note that the ALIGNN predictions used for prescreening were performed on structures generated from CDVAE prior to geometric relaxation with DFT. A full description of the DFT and ALIGNN (on the relaxed and unrelaxed structures) predictions is given in Table S1. To demonstrate how the predictive power of ALIGNN extrapolates from unrelaxed structures to relaxed structures for T_c predictions, we plot the ALIGNN T_c from the unrelaxed structures versus the ALIGNN T_c from the relaxed structures in Figure S2, where we observe that the predictions are relatively consistent between structures. We perform a similar analysis for formation energy and band gap in Figure S3 and Table S2. For E_{form}, we observe much closer agreement when comparing DFT and ALIGNN predictions for the relaxed (MAE of 0.15 eV/atom) structures compared to ALIGNN predictions for the unrelaxed (MAE of 0.42 eV/atom) structures (see Figure S3). With regard to band gap screening, for 41 of the materials we ran DFT for, DFT and ALIGNN predicted them to be metallic (in relaxed and unrelaxed configurations). For the remaining 20 structures, at least one of the three methods predicted a band gap (either DFT, ALIGNN on unrelaxed structures or ALIGNN on relaxed structures). A comparison of these band gap results is given in Table S2. The success of the ALIGNN prediction of T_c is a direct consequence of the availability of training data. In terms of deep learning models for material property prediction, 1058 structures are a relatively small amount of data on which to train on. The reason for the smaller training set size is due to the vast computational expense needed to perform these DFT calculations of the EPC properties. In principle, the ALIGNN prediction of T_c can be systematically improved by adding more DFT calculations to the training, which is an ongoing effort of JARVIS. We show the relationship between EPC parameters (λ, ω_{log}, T_c) for the 61 materials we performed DFT calculations for in Figure 3c and d. Figure 3c depicts an

https://doi.org/10.1021/acs.jpclett.3c01260
J. Phys. Chem. Lett. 2023, 14, 6630−6638

inverse relationship between λ and ω_{log}, and in Figure 3d, we observe a somewhat positive relationship between λ and T_c. These are typical behaviors of BCS superconductors and were observed in our work on BCS bulk and 2D superconductors.[6,7] From the colormap of Figure 3c and d, it is clear that a balance of high λ and ω_{log} is a necessary condition for a material to have a high T_c. It is important to note that our focus on ambient condition stoichiometric BCS superconductors significantly limits the value of T_c that can be achieved. High-pressure superconductors, non-stoichiometric (i.e., several cuprates and pnictides) superconductors, and unconventional superconductors (not mediated by electron−phonon interactions) can achieve much higher T_c than BCS superconductors. We hope to extend our workflow to these types of superconductors in the future, but for proof-of-concept and validation of our methods, we focus on BCS superconductors in this work.

The chemical composition, T_c, formation energy per atom, and energy above the convex hull of the top superconducting candidates are given in Table 1. As seen in the table, all of the 25 structures have negative formation energy. Although negative formation energy is a necessary prerequisite for thermodynamic stability, it does not guarantee thermodynamic stability. For this reason, we calculated the energy above the convex hull (shown in Table 1). We computed the convex hull of these structures from the formation energy calculations of the different phases in JARVIS-DFT. From here, we observed 15 structures within an energy of 0.45 eV or less from the convex hull and deem that these structures are the most likely to be experimentally synthesized. The atomic structures (all of P1 symmetry) of these 15 materials are given in Figure 4 (VN_2, MnN, VN, BN_2Zr, NP_2Sr, TaP_2, AlN_2Zr, NbRh, AlN_2V (I), TiO_2NbN, NBaP, ScO_3Zr, Al_2N, AlN_2V (II), TiN). The properties and atomic structures of all the materials we performed DFT verification forwill be available along with this manuscript. Although these 15 materials have an energy above the convex hull between 0.0 and 0.43 eV/atom, indicating that thermodynamic stability is still not guaranteed, they still may be synthesizable. In fact, Aykol et al.[61] demonstrated that nitride-based polymorphs with a higher energy above the convex hull can be stable up to a high energetic amorphous limit. Since a majority of these superconductors contain nitrogen, this gives promise that they can eventually be experimentally realized.

As a success metric of the CDVAE method for inverse design, it is important to measure how diverse the chemical composition and crystal structure of the generated materials are, not only with respect to the training data but with respect to larger areas of phase space. Out of the top 25 candidate superconductors, 20 do not have a chemical composition in the JARVIS training set used for CDVAE. Compounds with a stoichiometry of MnN, VN, AlN_2Zr, NbRh, and TiN are part of the training set and were all found to have superconducting phases in ref 6. Although these five candidates have similar chemistry to compounds in the training set, they all have entirely different crystal structures with the exception of NbRh (which has the same structure as JVASP-20529). Due to the fact that the JARVIS database has fewer materials (the primary focus of JARVIS is to expand the properties and accuracy of materials), we checked other well-established materials databases for these candidates. Specifically, we checked the Materials Project (over 150,000 structures) and the OQMD (over 1,000,000 structures). In addition, we searched the literature to see if any of these materials have been synthesized. For VN_2, we found three compounds in OQMD with entirely different structures (1239835, 1233906, 1589664) with E_{hull} ranging from 0.8 to 2.6 eV/atom. For Al_2N, we found four compounds in the OQMD with entirely different structures (1237731, 1415673, 1590028) with E_{hull} ranging from 0.9 to 2.6 eV/atom. We found 3 TaP_2 compounds (1372133, 1590238, 1237725) in the OQMD. The E_{hull} ranged from 0 to 1.2 eV/atom, but none of these phases resemble the structure in this study, which has a similar crystal structure to layered transition metal dichalcogenides (such as 2H-MoS_2). Upon searching the literature, we found that a semimetallic phase of TaP_2 had been recently synthesized[62] that possessed a different crystal structure than the superconducting phase reported in this work. This experimentally synthesized TaP_2 was found to possess quantum oscillations and nontrivial topological properties but was not found to be superconducting.[62] We found one AlN_2V compound in the Materials Project (mp-1247742), where the E_{hull} was 0.37 eV/atom. When comparing this structure to the two AlN_2V structures in our study, mp-1247742 has a similar form to AlN_2V (I) but a drastically different structure than AlN_2V (II). With regard to the five structures that have the same stoichiometry as structures in the training set, MnN, VN, NbRh, and TiN have multiple entries in the OQMD and Materials Project, while AlN_2Zr has just one entry in the Materials Project. Our NbRh structure is the same as OQMD 30785, 17746, 339226, mp-1963, and JVASP-20529 (our T_c is in agreement with the value obtained in ref 6), and our TiN structure is similar to the OQMD 1230416 entry. Upon searching the experimental literature, certain phases of TiN and VN have been reported to have superconducting properties.[63−66] We additionally searched the Supercon database (the Supercon database is unavailable as of December 2021, but previous papers have made this data set available for further research[67,68]), which consists of over 16,000 experimentally realized superconducting materials. We find no common materials among the top 25 CDVAE candidates and the Supercon database. This further proves that the CDVAE method can generate unique materials with a specific desired property covering previously undiscovered areas of phase space.

In this work, we used a multistep workflow, combining generative models, deep learning property prediction, and DFT to discover next-generation superconducting materials. We demonstrated that the deep learning property prediction using the ALIGNN model can accelerate the search for new superconductors by instantaneously screening the properties of the newly generated materials prior to DFT verification and experimental investigation. Our search revealed 25 newly predicted candidate superconductors, with 15 structures being close to the convex hull and T_c values as high as 20.2 K. Our approach goes beyond the standard funnel-like materials design workflow and allows for inverse design of novel materials, populating previously undiscovered areas of phase space.

■ ASSOCIATED CONTENT

Data Availability Statement

The data associated with the present work is available at https://figshare.com/articles/dataset/Inverse_Design_of_Next-Generation_Superconductors_Using_Data-Driven_Deep_Generative_Models/23681025.

https://doi.org/10.1021/acs.jpclett.3c01260
J. Phys. Chem. Lett. 2023, 14, 6630−6638

Supporting Information

The Supporting Information is available free of charge at https://pubs.acs.org/doi/10.1021/acs.jpclett.3c01260.

CDVAE loss function, tabulated data for relaxed and unrelaxed structures computed with ALIGNN and DFT, and additional comparisons of ALIGNN for relaxed and unrelaxed structures (PDF)

AUTHOR INFORMATION

Corresponding Author

Daniel Wines − *Material Measurement Laboratory, National Institute of Standards and Technology, Gaithersburg, Maryland 20899, United States;* orcid.org/0000-0003-3855-3754; Email: daniel.wines@nist.gov

Authors

Tian Xie − *Microsoft Research AI4Science, Cambridge, United Kingdom CB1 2FB*

Kamal Choudhary − *Material Measurement Laboratory, National Institute of Standards and Technology, Gaithersburg, Maryland 20899, United States; DeepMaterials LLC, Silver Spring, Maryland 20906, United States;* orcid.org/0000-0001-9737-8074

Complete contact information is available at: https://pubs.acs.org/10.1021/acs.jpclett.3c01260

Notes

The authors declare no competing financial interest.
Software packages mentioned in the article can be found at https://github.com/usnistgov/jarvis, https://github.com/knc6/cdvae, and https://github.com/txie-93/cdvae.

ACKNOWLEDGMENTS

All authors thank the National Institute of Standards and Technology for funding, computational, and data-management resources, specifically the NIST Nisaba and Raritan HPC clusters. K.C. thanks XSEDE (Extreme Science and Engineering Discovery Environment) for computational resources and support under allocation number TG-DMR 190095. Contributions from K.C. were supported by the financial assistance award 70NANB19H117 from the U.S. Department of Commerce, National Institute of Standards and Technology.

REFERENCES

(1) Onnes, H. K. The resistance of pure mercury at helium temperatures. *Commun. Phys. Lab. Univ. Leiden, b* **1911**, *120*.

(2) Poole, C. P.; Farach, H. A.; Creswick, R. J. *Superconductivity*; Academic Press: 2013.

(3) Rogalla, H.; Kes, P. H. *100 years of superconductivity*; Taylor & Francis: 2011.

(4) Cooper, L. N.; Feldman, D. *BCS: 50 years*; World Scientific: 2010.

(5) Giustino, F. Electron-phonon interactions from first principles. *Rev. Mod. Phys.* **2017**, *89*, 015003.

(6) Choudhary, K.; Garrity, K. Designing high-TC superconductors with BCS-inspired screening, density functional theory, and deep-learning. *npj Computational Materials* **2022**, *8*, 244.

(7) Wines, D.; Choudhary, K.; Biacchi, A. J.; Garrity, K. F.; Tavazza, F. High-throughput DFT-based discovery of next generation two-dimensional (2D) superconductors. *Nano Lett.* **2023**, *23*, 969−978.

(8) Shipley, A. M.; Hutcheon, M. J.; Needs, R. J.; Pickard, C. J. High-throughput discovery of high-temperature conventional superconductors. *Phys. Rev. B* **2021**, *104*, 054501.

(9) García-Nieto, P. J.; García-Gonzalo, E.; Paredes-Sánchez, J. Prediction of the critical temperature of a superconductor by using the WOA/MARS, Ridge, Lasso and Elastic-net machine learning techniques. *Neural Computing and Applications* **2021**, *33*, 17131−17145.

(10) Stanev, V.; Oses, C.; Kusne, A. G.; Rodriguez, E.; Paglione, J.; Curtarolo, S.; Takeuchi, I. Machine learning modeling of superconducting critical temperature. *npj Computational Materials* **2018**, *4*, 29.

(11) Zhang, J.; Zhu, Z.; Xiang, X. D.; Zhang, K.; Huang, S.; Zhong, C.; Qiu, H.-J.; Hu, K.; Lin, X. Machine learning prediction of superconducting critical temperature through the structural descriptor. *J. Phys. Chem. C* **2022**, *126*, 8922−8927.

(12) Meredig, B.; Antono, E.; Church, C.; Hutchinson, M.; Ling, J.; Paradiso, S.; Blaiszik, B.; Foster, I.; Gibbons, B.; Hattrick-Simpers, J.; Mehta, A.; Ward, L. Can machine learning identify the next high-temperature superconductor? Examining extrapolation performance for materials discovery. *Mol. Syst. Des. Eng.* **2018**, *3*, 819−825.

(13) Roter, B.; Dordevic, S. Predicting new superconductors and their critical temperatures using machine learning. *Physica C: Superconductivity and its Applications* **2020**, *575*, 1353689.

(14) Menon, D.; Ranganathan, R. A generative approach to materials discovery, design, and optimization. *ACS Omega* **2022**, *7*, 25958−25973.

(15) Jain, A.; Ong, S. P.; Hautier, G.; Chen, W.; Richards, W. D.; Dacek, S.; Cholia, S.; Gunter, D.; Skinner, D.; Ceder, G.; Persson, K. A. Commentary: The Materials Project: A materials genome approach to accelerating materials innovation. *APL Materials* **2013**, *1*, 011002.

(16) Saal, J. E.; Kirklin, S.; Aykol, M.; Meredig, B.; Wolverton, C. Materials design and discovery with high-throughput density functional theory: The Open Quantum Materials Database (OQMD). *JOM* **2013**, *65*, 1501−1509.

(17) Kirklin, S.; Saal, J. E.; Meredig, B.; Thompson, A.; Doak, J. W.; Aykol, M.; Rühl, S.; Wolverton, C. The Open Quantum Materials Database (OQMD): assessing the accuracy of DFT formation energies. *npj Computational Materials* **2015**, *1*, 15010.

(18) Haastrup, S.; Strange, M.; Pandey, M.; Deilmann, T.; Schmidt, P. S.; Hinsche, N. F.; Gjerding, M. N.; Torelli, D.; Larsen, P. M.; Riis-Jensen, A. C.; Gath, J.; Jacobsen, K. W.; Mortensen, J. J.; Olsen, T.; Thygesen, K. S. The Computational 2D Materials Database: high-throughput modeling and discovery of atomically thin crystals. *2D Materials* **2018**, *5*, 042002.

(19) Gjerding, M. N.; et al. Recent progress of the Computational 2D Materials Database (C2DB). *2D Materials* **2021**, *8*, 044002.

(20) Choudhary, K.; Garrity, K. F.; Reid, A. C.; DeCost, B.; Biacchi, A. J.; Hight Walker, A. R.; Trautt, Z.; Hattrick-Simpers, J.; Kusne, A. G.; Centrone, A.; et al. The joint automated repository for various integrated simulations (JARVIS) for data-driven materials design. *npj Computational Materials* **2020**, *6*, 173.

(21) Ong, S. P.; Richards, W. D.; Jain, A.; Hautier, G.; Kocher, M.; Cholia, S.; Gunter, D.; Chevrier, V. L.; Persson, K. A.; Ceder, G. Python Materials Genomics (pymatgen): A robust, open-source python library for materials analysis. *Comput. Mater. Sci.* **2013**, *68*, 314−319.

(22) Ramesh, A.; Pavlov, M.; Goh, G.; Gray, S.; Voss, C.; Radford, A.; Chen, M.; Sutskever, I. Zero-shot text-to-image generation; 2021; https://arxiv.org/abs/2102.12092.

(23) Wu, K. E.; Yang, K. K.; van den Berg, R.; Zou, J. Y.; Lu, A. X.; Amini, A. P. Protein structure generation via folding diffusion; 2022; https://arxiv.org/abs/2209.15611.

(24) Xie, T.; Fu, X.; Ganea, O.-E.; Barzilay, R.; Jaakkola, T. Crystal diffusion variational autoencoder for periodic material generation; 2021; https://arxiv.org/abs/2110.06197.

(25) Lyngby, P.; Thygesen, K. S. Data-driven discovery of 2D materials by deep generative models. *npj Computational Materials* **2022**, *8*, 232.

(26) Moustafa, H.; Lyngby, P. M.; Mortensen, J. J.; Thygesen, K. S.; Jacobsen, K. W. Hundreds of new, stable, one-dimensional materials

from a generative machine learning model. *Phys. Rev. Mater.* **2023**, *7*, 014007.
(27) Fung, V.; Jia, S.; Zhang, J.; Bi, S.; Yin, J.; Ganesh, P. Atomic structure generation from reconstructing structural fingerprints. *Machine Learning: Science and Technology* **2022**, *3*, 045018.
(28) Noh, J.; Gu, G. H.; Kim, S.; Jung, Y. Machine-enabled inverse design of inorganic solid materials: promises and challenges. *Chem. Sci.* **2020**, *11*, 4871−4881.
(29) Kim, S.; Noh, J.; Gu, G. H.; Aspuru-Guzik, A.; Jung, Y. Generative adversarial networks for crystal structure prediction. *ACS Central Science* **2020**, *6*, 1412−1420.
(30) Long, T.; Fortunato, N. M.; Opahle, I.; Zhang, Y.; Samathrakis, I.; Shen, C.; Gutfleisch, O.; Zhang, H. Constrained crystals deep convolutional generative adversarial network for the inverse design of crystal structures. *npj Computational Materials* **2021**, *7*, 66.
(31) Song, Y.; Siriwardane, E. M. D.; Zhao, Y.; Hu, J. Computational discovery of new 2D materials using deep learning generative models. *ACS Appl. Mater. Interfaces* **2021**, *13*, 53303−53313.
(32) Noh, J.; Kim, J.; Stein, H. S.; Sanchez-Lengeling, B.; Gregoire, J. M.; Aspuru-Guzik, A.; Jung, Y. Inverse design of solid-state materials via a continuous representation. *Matter* **2019**, *1*, 1370−1384.
(33) Zhao, Y.; Al-Fahdi, M.; Hu, M.; Siriwardane, E. M. D.; Song, Y.; Nasiri, A.; Hu, J. High-throughput discovery of novel cubic crystal materials using deep generative neural networks. *Advanced Science* **2021**, *8*, 2100566.
(34) Ren, Z.; et al. An invertible crystallographic representation for general inverse design of inorganic crystals with targeted properties. *Matter* **2022**, *5*, 314−335.
(35) Kingma, D. P.; Welling, M. Auto-encoding variational bayes; 2013; https://arxiv.org/abs/1312.6114.
(36) Sohl-Dickstein, J.; Weiss, E.; Maheswaranathan, N.; Ganguli, S. Deep unsupervised learning using nonequilibrium thermodynamics. Proceedings of the 32nd International Conference on Machine Learning, Lille, France, 2015; pp 2256−2265.
(37) Song, Y.; Ermon, S. Generative modeling by estimating gradients of the data distribution; 2019; https://arxiv.org/abs/1907.05600.
(38) Sohl-Dickstein, J.; Weiss, E. A.; Maheswaranathan, N.; Ganguli, S. Deep unsupervised learning using nonequilibrium thermodynamics; 2015; https://arxiv.org/abs/1503.03585.
(39) Batzner, S.; Musaelian, A.; Sun, L.; Geiger, M.; Mailoa, J. P.; Kornbluth, M.; Molinari, N.; Smidt, T. E.; Kozinsky, B. E. (3)-equivariant graph neural networks for data-efficient and accurate interatomic potentials. *Nat. Commun.* **2022**, *13*, 2453.
(40) Choudhary, K.; DeCost, B. Atomistic Line Graph Neural Network for improved materials property predictions. *npj Computational Materials* **2021**, *7*, 185.
(41) Wang, M.; Yu, L.; Zheng, D.; Gan, Q.; Gai, Y.; Ye, Z.; Li, M.; Zhou, J.; Huang, Q.; Ma, C., et al. Deep Graph Library: Towards efficient and scalable deep learning on graphs. arXiv e-prints; 2019.
(42) Paszke, A.; Gross, S.; Massa, F.; Lerer, A.; Bradbury, J.; Chanan, G.; Killeen, T.; Lin, Z.; Gimelshein, N.; Antiga, L.; et al. Pytorch: An imperative style, high-performance deep learning library. *Advances in neural information processing systems* **2019**, *32*, 8026−8037.
(43) Choudhary, K.; Zhang, Q.; Reid, A. C.; Chowdhury, S.; Van Nguyen, N.; Trautt, Z.; Newrock, M. W.; Congo, F. Y.; Tavazza, F. Computational screening of high-performance optoelectronic materials using OptB88vdW and TB-mBJ formalisms. *Scientific data* **2018**, *5*, 180082.
(44) Choudhary, K.; Bercx, M.; Jiang, J.; Pachter, R.; Lamoen, D.; Tavazza, F. Accelerated discovery of efficient solar cell materials using quantum and machine-learning methods. *Chem. Mater.* **2019**, *31*, 5900−5908.
(45) Choudhary, K.; Garrity, K. F.; Ghimire, N. J.; Anand, N.; Tavazza, F. High-throughput search for magnetic topological materials using spin-orbit spillage, machine learning, and experiments. *Phys. Rev. B* **2021**, *103*, 155131.
(46) Choudhary, K.; Garrity, K. F.; Tavazza, F. High-throughput discovery of topologically non-trivial materials using spin-orbit spillage. *Sci. Rep.* **2019**, *9*, 8534.
(47) Choudhary, K.; Garrity, K. F.; Jiang, J.; Pachter, R.; Tavazza, F. Computational search for magnetic and non-magnetic 2D topological materials using unified spin−orbit spillage screening. *NPJ. Computational Materials* **2020**, *6*, 49.
(48) Choudhary, K.; Cheon, G.; Reed, E.; Tavazza, F. Elastic properties of bulk and low-dimensional materials using van der Waals density functional. *Phys. Rev. B* **2018**, *98*, 014107.
(49) Choudhary, K.; Garrity, K. F.; Sharma, V.; Biacchi, A. J.; Hight Walker, A. R.; Tavazza, F. High-throughput density functional perturbation theory and machine learning predictions of infrared, piezoelectric, and dielectric responses. *NPJ. Computational Materials* **2020**, *6*, 64.
(50) Choudhary, K.; Ansari, J. N.; Mazin, I. I.; Sauer, K. L. Density functional theory-based electric field gradient database. *Scientific Data* **2020**, *7*, 362.
(51) Choudhary, K.; Kalish, I.; Beams, R.; Tavazza, F. High-throughput identification and characterization of two-dimensional materials using density functional theory. *Sci. Rep.* **2017**, *7*, 5179.
(52) Wines, D.; Choudhary, K.; Tavazza, F. Systematic DFT+U and Quantum Monte Carlo benchmark of magnetic two-dimensional (2D) CrX3 (X = I, Br, Cl, F). *J. Phys. Chem. C* **2023**, *127*, 1176−1188.
(53) Choudhary, K.; Tavazza, F. Convergence and machine learning predictions of Monkhorst-Pack k-points and plane-wave cut-off in high-throughput DFT calculations. *Computational materials science* **2019**, *161*, 300−308.
(54) Baroni, S.; Giannozzi, P.; Testa, A. Green's-function approach to linear response in solids. *Physical review letters* **1987**, *58*, 1861.
(55) Gonze, X. Perturbation expansion of variational principles at arbitrary order. *Phys. Rev. A* **1995**, *52*, 1086.
(56) Wierzbowska, M.; de Gironcoli, S.; Giannozzi, P. Origins of low-and high-pressure discontinuities of T_c in niobium; 2005; https://arxiv.org/abs/cond-mat/0504077.
(57) Giannozzi, P.; Baroni, S.; Bonini, N.; Calandra, M.; Car, R.; Cavazzoni, C.; Ceresoli, D.; Chiarotti, G. L.; Cococcioni, M.; Dabo, I.; et al. QUANTUM ESPRESSO: a modular and open-source software project for quantum simulations of materials. *J. Phys.: Condens. Matter* **2009**, *21*, 395502.
(58) Perdew, J. P.; Ruzsinszky, A.; Csonka, G. I.; Vydrov, O. A.; Scuseria, G. E.; Constantin, L. A.; Zhou, X.; Burke, K. Restoring the density-gradient expansion for exchange in solids and surfaces. *Physical review letters* **2008**, *100*, 136406.
(59) Garrity, K. F.; Bennett, J. W.; Rabe, K. M.; Vanderbilt, D. Pseudopotentials for high-throughput DFT calculations. *Comput. Mater. Sci.* **2014**, *81*, 446−452.
(60) McMillan, W. Transition temperature of strong-coupled superconductors. *Phys. Rev.* **1968**, *167*, 331.
(61) Aykol, M.; Dwaraknath, S. S.; Sun, W.; Persson, K. A. Thermodynamic limit for synthesis of metastable inorganic materials. *Science Advances* **2018**, *4*, No. eaaq0148.
(62) Wang, H.; Su, H.; Zhang, J.; Xia, W.; Lin, Y.; Liu, X.; Hou, X.; Yu, Z.; Yu, N.; Wang, X.; Zou, Z.; Wang, Y.; Liang, Q.; Zhen, Y.; Guo, Y. Quantum oscillations and nontrivial topological state in a compensated semimetal TaP_2. *Phys. Rev. B* **2019**, *100*, 115127.
(63) Pan, V.; Prokhorov, V.; Komashko, V.; Kaminsky, G.; Kousenetsov, M.; Tretiatchenko, C. Superconducting properties of TaN and VN films. *IEEE Trans. Magn.* **1989**, *25*, 2000−2003.
(64) Romanov, N. R.; Zolotov, P. I.; Vakhtomin, Y. B.; Divochiy, A. V.; Smirnov, K. V. Electron diffusivity measurements of VN superconducting single-photon detectors. *Journal of Physics: Conference Series* **2018**, *1124*, 051032.
(65) Saveskul, N.; Titova, N.; Baeva, E.; Semenov, A.; Lubenchenko, A.; Saha, S.; Reddy, H.; Bogdanov, S.; Marinero, E.; Shalaev, V.; Boltasseva, A.; Khrapai, V.; Kardakova, A.; Goltsman, G. Superconductivity behavior in epitaxial TiN films points to surface magnetic disorder. *Phys. Rev. Appl.* **2019**, *12*, 054001.

(66) Jaim, H. M. I.; Aguilar, J. A.; Sarabi, B.; Rosen, Y. J.; Ramanayaka, A. N.; Lock, E. H.; Richardson, C. J. K.; Osborn, K. D. Superconducting TiN films sputtered over a large range of substrate DC bias. *IEEE Transactions on Applied Superconductivity* **2015**, *25*, 1−5.
(67) vstanev1, Supercon; 2021; https://github.com/vstanev1/Supercon.
(68) Hamidieh, K. A data-driven statistical model for predicting the critical temperature of a superconductor. *Comput. Mater. Sci.* **2018**, *154*, 346−354.

https://doi.org/10.1021/acs.jpclett.3c01260
J. Phys. Chem. Lett. 2023, 14, 6630−6638